Journal of ELECTRONIC MATERIALS, Vol. 39, No. 7, 2010
DOI: 10.1007/s11664-010-1086-7

Investigation of Multicarrier Transport in LPE-Grown $Hg_{1-x}Cd_xTe$ Layers

G.A. UMANA-MEMBRENO,[1,4] J. ANTOSZEWSKI,[1] L. FARAONE,[1] E.P.G.SMITH,[2] G.M. VENZOR,[2] S.M. JOHNSON,[2] and V. PHILLIPS[3]

1.—School of Electrical, Electronic and Computer Engineering, The University of Western Australia, Crawley, WA 6009, Australia. 2.—Raytheon Visions Systems, Goleta, CA 93117, USA. 3.—Raytheon Australia, Henderson, WA 6166, Australia. 4.—e-mail: umana-ga@ee.uwa.edu.au

A detailed study is presented of multicarrier transport properties in liquid-phase epitaxy (LPE)-grown *n*-type HgCdTe films using advanced mobility spectrum analysis techniques over the temperature range from 95 K to 300 K. Three separate electron species were identified that contribute to the total conduction, and the temperature-dependent characteristics of carrier concentration and mobility were extracted for each individual carrier species. Detailed analysis allows the three observed contributions to be assigned to carriers located in the bulk long-wave infrared (LWIR) absorbing layer, the wider-gap substrate/HgCdTe transition layer, and a surface accumulation layer. The activation energy of the dominant high-mobility LWIR bulk carrier concentration in the high temperature range gives a very good fit to the Hansen and Schmit expression for intrinsic carrier concentration in HgCdTe with a bandgap of 172 meV. The mobility of these bulk electrons follows the classic $\mu \sim T^{-3/2}$ dependence for the phonon scattering regime. The much lower sheet densities found for the other two, lower-mobility electron species show activation energies of the order of ~20 meV, and mobilities that are only weakly dependent on temperature and consistent with expected values for the wider-bandgap transition layer and a surface accumulation layer.

Key words: HgCdTe, quantitative mobility spectrum analysis (QMSA), Hall effect, electronic transport, multiple carrier transport, high-resolution QMSA, surface accumulation

INTRODUCTION

Third-generation infrared detector arrays employ complex, multilayer, epitaxially grown HgCdTe structures.[1] The growth and optimization of such material represents a serious challenge and, hence, information on transport properties is crucial to provide feedback to the growth process. The extraction of transport properties in semiconductors usually involves Hall and resistivity measurements, often using temperature-dependent, and more recently magnetic-field-dependent, techniques. In a semiconductor material with only one carrier present (single conduction mechanism) the analysis of the Hall and resistivity data is straightforward. However, if more than one carrier species is involved, the analysis becomes much more complex. In the case of multilayer structures one can expect not only conduction mechanisms related to bulk or surface mechanisms, which are usually present in a single layer, but also contributions from all layers in the structure. Originally, in order to deal with this complexity, the multicarrier fitting procedure was employed.[2] However, this approach is totally inadequate when applied to modern multilayer structures. As a natural evolution of the multicarrier fitting procedure, new approaches have been proposed based on transformation of the Hall and resistivity data into conductivity versus

(Received September 29, 2009; accepted January 7, 2010; published online February 11, 2010)

mobility spectra.[3] Over the last two decades the mobility spectrum technique has been enhanced and developed into a practical tool, with contributions from numerous researchers.[4–9] In this work, two different quantitative mobility spectrum analysis (QMSA) algorithms have been employed in the analysis of measured magnetic-field-dependent sheet resistivity and Hall-coefficient data: a commercially available version of improved quantitative mobility spectrum analysis (iQMSA),[8] and a recently developed high-resolution mobility spectrum analysis procedure that represents a significant advance in this area.[10]

EXPERIMENTAL PROCEDURES

An in-doped n-type HgCdTe wafer was grown at Raytheon Vision Systems by standard Hg-rich vertical liquid-phase epitaxy (LPE) on a lattice-matched CdZnTe substrate, which is typically used for the growth of second-generation double-layer heterojunction detector architectures for the long-wave infrared (LWIR) range.[11] Three nominally identical HgCdTe samples originating from the above-mentioned wafer, denoted R2A, R3A, and R3B, were used for fabrication of Hall devices at The University of Western Australia (UWA). Test structures with van der Pauw configuration were mesa-etched in the 20-μm-thick epilayers using 0.5% Br/HBr solution in the shape of a Greek cross with an arm length and width of 400 μm and 200 μm, respectively. Ohmic contacts to the ends of the arms were fabricated using thermally evaporated indium. The maximum processing temperature was limited to 105°C. The resistivity and Hall-effect measurements were performed as a function of magnetic field intensity from 0 T to 2 T, using a narrow-gap electromagnet (1 cm gap), at sample temperatures from 95 K to 300 K in a liquid-nitrogen-cooled continuous-flow cryostat.

EXPERIMENTAL DATA ANALYSIS

The longitudinal and transverse conductivity tensor components, $\sigma_{xx}(B)$ and $\sigma_{xy}(B)$, respectively, were obtained from the measured magnetic-field-dependent sheet resistance $R_S(B)$ and Hall coefficient $R_H(B)$ using the following expressions[3]:

$$\sigma_{xx}(B) = \frac{1}{R_s(B)\left[1 + \left(\frac{R_H(B)B}{R_s(B)}\right)^2\right]},$$

$$\sigma_{xy} = \frac{R_H(B)B}{R_s^2(B)\left[1 + \left(\frac{R_H(B)B}{R_s(B)}\right)^2\right]}.$$

In the presence of multiple carriers—or more generally, a distribution of carriers—the contribution of all carriers to the conductivity tensors is described by the mobility transforms[8]:

$$\sigma_{xx}(B) = \int_0^\infty \frac{s_p(\mu) + s_n(\mu)}{1 + \mu^2 B^2}\,\mathrm{d}\mu \approx \sum_{i=1}^{N} \frac{S_p(\mu_i) + S_n(\mu_i)}{1 + \mu_i^2 B^2},$$

$$\sigma_{xy}(B) = \int_0^\infty \frac{\left[s_p(\mu) - s_n(\mu)\right]\mu B}{1 + \mu^2 B^2}\,\mathrm{d}\mu \approx \sum_{i=1}^{N} \frac{\left[S_p(\mu_i) - S_n(\mu_i)\right]\mu B}{1 + \mu_i^2 B^2},$$

where $s_p(\mu)$ and $s_n(\mu)$ are the hole and electron mobility-conductivity density functions, respectively, and $S_p(\mu)$ and $S_n(\mu)$ are referred to as the hole and electron mobility spectra, respectively, which are extracted numerically from the measured conductivity tensor components using mobility spectrum analysis algorithms.

In this work, the longitudinal and transverse conductivity tensor components were analyzed using two different algorithms: Lake Shore Cryotronics' commercial iQMSA technique and a newly developed high-resolution mobility spectrum analysis (HR-QMSA) procedure.[10] Since the new HR-QMSA does not utilize the derivatives of the measured conductivity tensor components, it is less sensitive to noise in the measured data and, thus, it is more robust and has shown much greater resolution than iQMSA. Furthermore, HR-QMSA does not require *a priori* interpolation or smoothing of experimental data. In contrast to iQMSA,[8] HR-QMSA operates through modification of the whole electron and hole spectra at every iteration, and yields smooth spectra without the need for point-swapping procedures. However, HR-QMSA is computationally more intensive than iQMSA; for a typical analysis requiring ~10,000 iterations for convergence to minimum error, the algorithm runtime approaches 5 h on a computer with a 2-GHz Pentium IV processor and 2 GB of memory. Although further refinements and optimizations may be required to reduce computation time, the HR-QMSA algorithm has undergone extensive testing employing synthetic data sets with varying degrees of complexity and noise levels, in addition to those published previously that were used to benchmark iQMSA. These tests have demonstrated that HR-QMSA is able to better resolve closely spaced mobility peaks arising from separate carriers, and provides more accurate information than iQMSA on the spread and distribution of the mobility for each individual carrier species. This is demonstrated in Fig. 1, where the resolution of HR-QMSA is evaluated against iQMSA using a synthetic conductivity tensor data set with 1% added random noise. The synthetic data set is

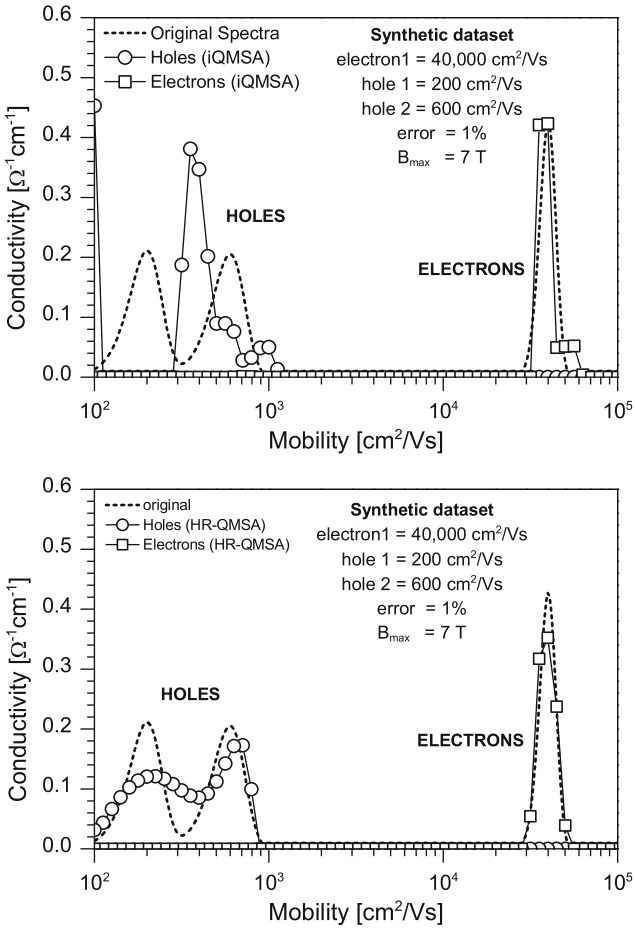

Fig. 1. Resolution evaluation of iQMSA (top) and HR-QMSA (bottom) mobility spectrum analysis algorithms using synthetic data with 1% added random error. Note that HR-QMSA exhibits superior line-width resolution and the ability to separate the two low-mobility hole peaks. The synthetic data set is identical to that originally employed in Ref. 8 to assess the performance of iQMSA.

identical to that originally employed in Ref. 8 to assess the performance of iQMSA.

RESULTS AND DISCUSSION

Figures 2 and 3 show electron mobility spectra obtained for the three investigated samples using the iQMSA and HR-QMSA algorithms, respectively. Although the general shapes of the corresponding spectra are similar for both cases, HR-QMSA consistently demonstrates better conductivity peak resolution as well as better definition of broadening effects. The HR-QMSA spectra also demonstrate much more robust evolutionary trends versus temperature, making the peak identification and analysis much more consistent and robust. This is particularly evident from the more detailed expanded spectra at 125 K shown in Fig. 4, which were obtained by iQMSA and HR-QMSA and are taken from the same data set as that shown in Figs. 2 and 3. The separation of peaks E1 and E2 is clearly visible only in the HR-QMSA spectrum. This

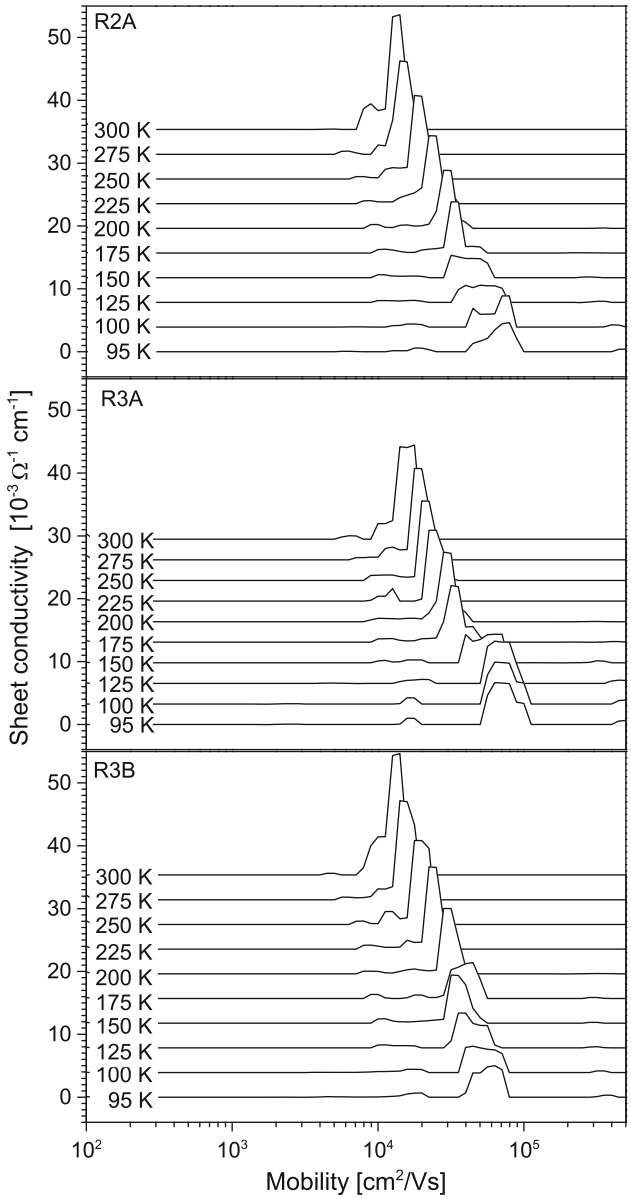

Fig. 2. iQMSA electron mobility spectra for the three investigated samples at different temperatures.

ability to separate closely spaced mobility peaks represents a significant milestone in the development of the mobility spectrum technique, since it overcomes some of the limitations of iQMSA and allows for greater insight into the properties of multilayered and/or multicarrier structures. Consequently, all additional experimental data analysis presented in this paper has been undertaken using only HR-QMSA.

In this paper only electron spectra have been analyzed, since no hole species were observed in the spectra for all samples under all experimental conditions. As evident from Fig. 3 the HR-QMSA spectra for all three samples are very similar, indicating excellent uniformity across the wafer. All samples were found to contain three carriers,

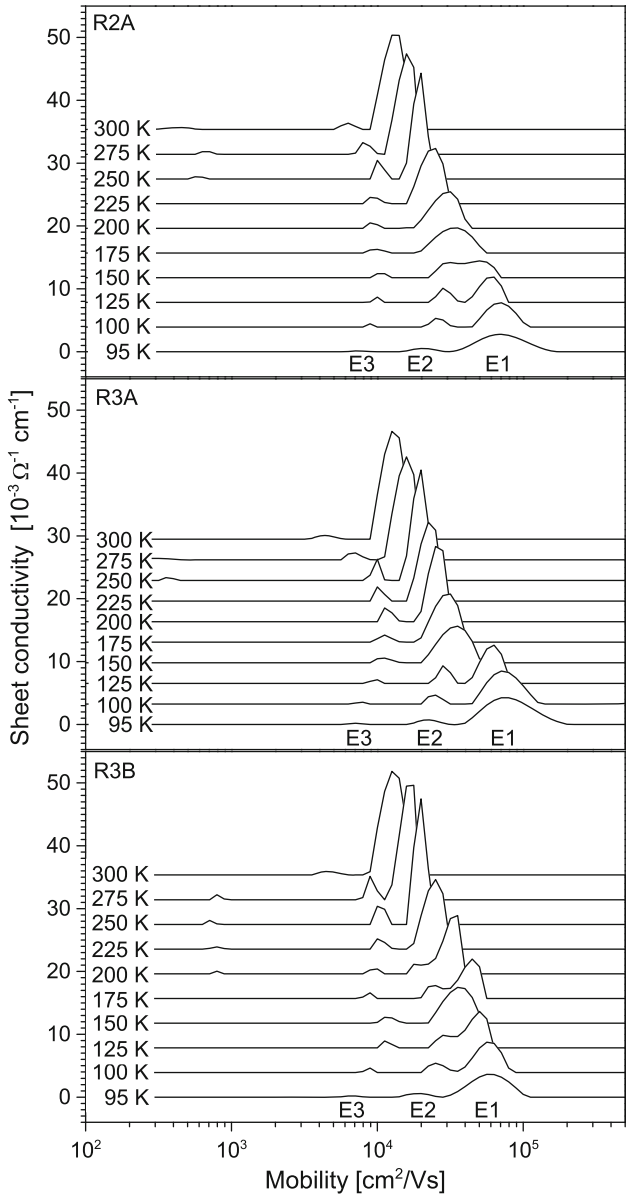

Fig. 3. HR-QMSA electron mobility spectra for the three investigated samples at different temperatures. The three identified electron species are labeled E1, E2, and E3.

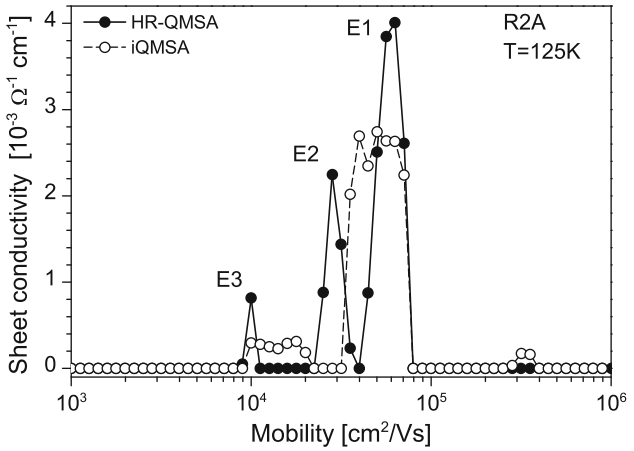

Fig. 4. Comparison of the peak-resolving capabilities of iQMSA and HR-QMSA for the same data set at 125 K.

labeled E1, E2, and E3, with all spectra being dominated by conduction contributions from the high-mobility peak E1. It is interesting to observe that this dominant electron peak, E1, splits into two clearly resolved peaks, E1 and E2, at temperatures below 150 K. The lower-mobility third peak, E3, remains clearly visible over the entire temperature range. It is also important to note that the split of peak E1 into peaks E1 and E2 at lower temperatures is not resolved by iQMSA (see Fig. 2 and details in Fig. 4).

The carrier concentration and mobility for each conductivity contribution (peak) were extracted from the spectra of respective samples as a function of temperature. Figure 5 shows the concentration of electrons represented by the E1, E2, and E3 peaks for the three investigated samples. The dominant electron peak E1 (62% contribution to the total conductivity at 95 K) shows thermal activation of intrinsic carriers at high temperatures with an activation energy of 174 meV, 163 meV, and 180 meV for samples R2A, R3A, and R3B, respectively. Taking into account the experimental error of approximately ±20 meV, these values represent an average value of 172 meV, which is typical for LWIR HgCdTe material. At lower temperatures the E1 concentration saturates at around 1×10^{15} cm^{-3}, in agreement with the nominal indium extrinsic doping level in this material.[11] This temperature-dependent behavior is typical for bulk electrons in *n*-type HgCdTe LWIR material and, hence, the carrier concentration has been expressed per unit volume (left-hand scale in Fig. 5). The contributions of carriers represented by peaks E2 and E3 were 32% and 6% of the total conductivity at 95 K, respectively. Both these carriers demonstrate thermal activation with practically the same activation energy between 20 meV and 26 meV for all three samples, with E2 having about 50% higher sheet density. Consequently, the E2 and E3 electron species can be tentatively assigned to the higher-*x*-value HgCdTe/substrate transition layer and the surface accumulation layer, respectively. Since the location and thickness of these layers are not known precisely, the concentrations of E2 and E3 are expressed as sheet density per unit area (right-hand scale in Fig. 5).

The temperature dependence of the mobility for each of the three observed electron species is shown in Fig. 6 for the three investigated samples. The E1 electrons, in all three samples, demonstrate the classic $\sim T^{-3/2}$ dependence, as expected for bulk electrons in the temperature range dominated by phonon scattering, and have a mobility approaching 10^5 cm^2/Vs at low temperatures, which is indicative of very high-quality material. Electron species E2 and E3 demonstrate a much weaker temperature

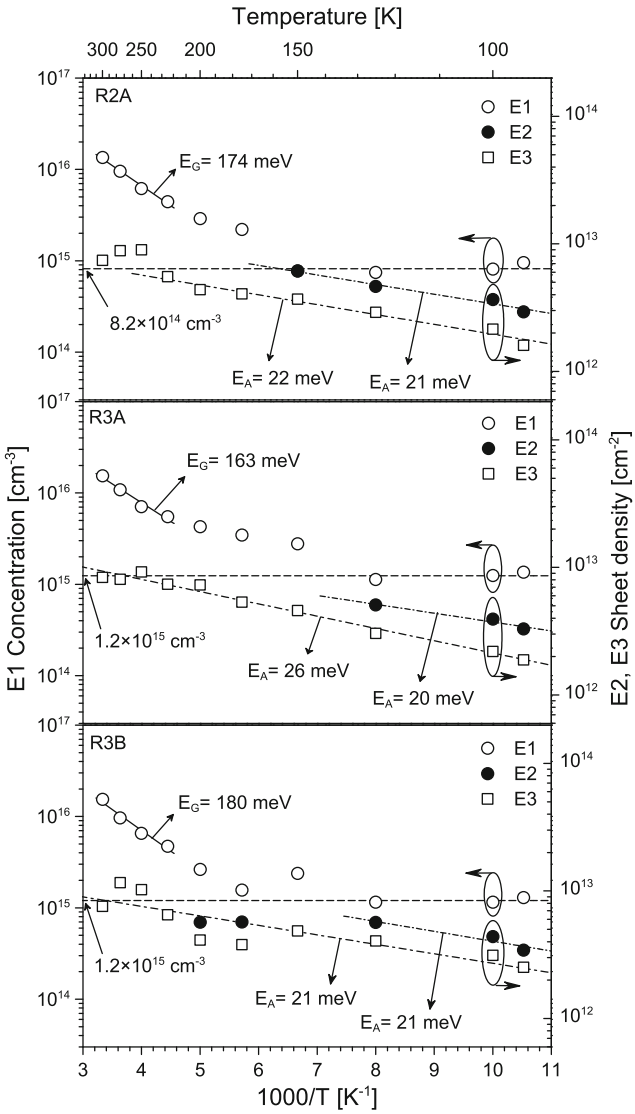

Fig. 5. Temperature-dependent electron concentration characteristics for the three identified carriers: E1, E2, and E3. Activation energies were obtained using a straight-line fit to the data.

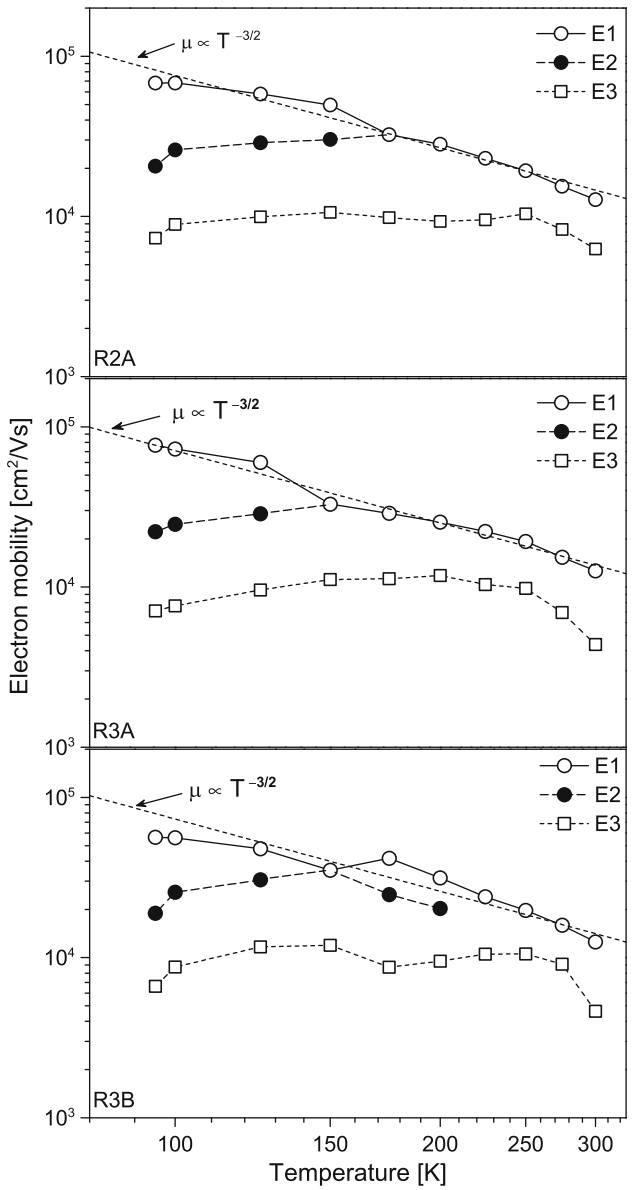

Fig. 6. Temperature-dependent electron mobility profiles for the three identified carriers.

dependence and very similar shape over the whole temperature range. The E2 electron species, which is only evident at temperatures below 150 K, has a maximum mobility close to 3×10^4 cm^2/Vs, whereas the maximum mobility of the E3 electrons is about 10^4 cm^2/Vs.

A detailed analysis of the concentration of the dominant electron species E1 for temperatures above 200 K is presented in Fig. 7. Fitting the data to the Hansen and Schmit formula for the intrinsic carrier concentration in HgCdTe,[12] which takes into account the temperature dependence of the bandgap, yields Cd mole fractions of x = 0.239, 0.234, and 0.237 for samples R2A, R3A, and R3B, respectively. Taking into account the experimental error of approximately ±0.003, these x-values are very similar, with an average alloy composition of x = 0.237. Once again, these values are indicative of very uniform material, especially given that only four experimental data points were used to fit the Hansen and Schmit formula. These parameters, and other transport parameters extracted during the course of this study, are presented in Table I.

The mobility differences evident in Fig. 6 between the E2 and E3 electron species indicate that the E3 electrons are located in a region of the sample with stronger scattering mechanisms than are the E2 electrons. Since the mobility of E2 electrons approaches the mobility level demonstrated by the high-mobility E1 bulk electrons, they can be assumed to be physically located in a higher-quality region of the sample, possibly at or near the HgCdTe/substrate interface or even within the wider-bandgap HgCdTe transition region close to

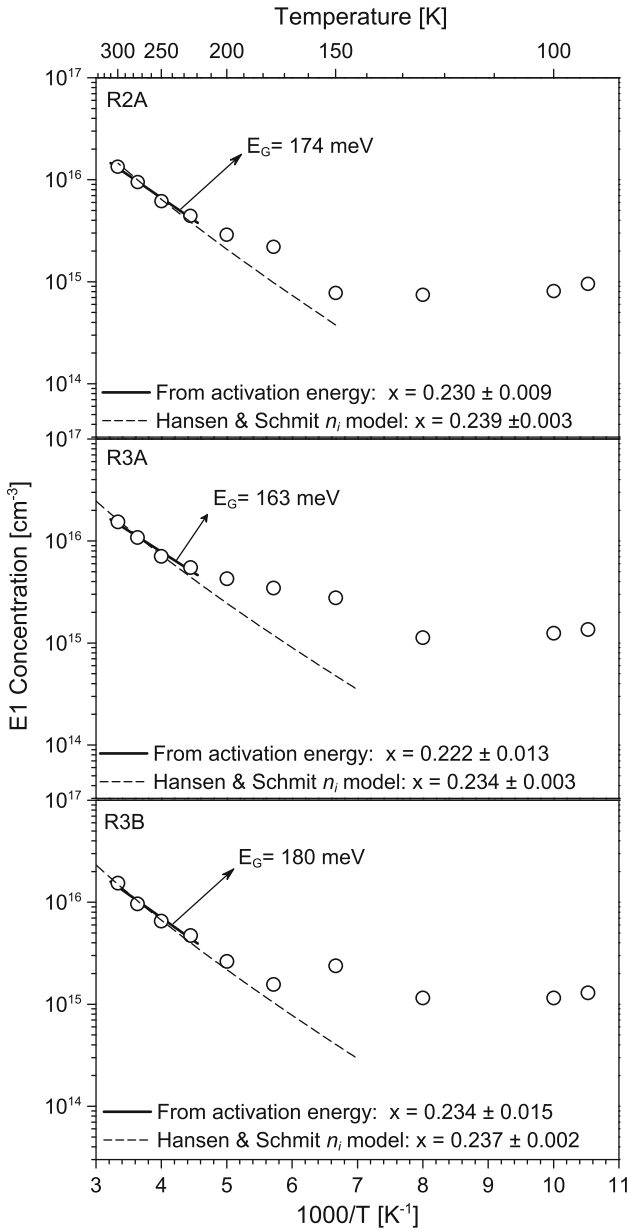

Fig. 7. Composition analysis using the Hansen and Schmit[12] expression in the intrinsic region.

the substrate. The E3 electrons can be assigned to a surface accumulation layer, since the observed sheet density and mobility are consistent with a number of previous studies of electron accumulation and/or inversion layers in HgCdTe. This interpretation is also supported by a comparison of the sheet densities of the E2 and E3 electrons. Assuming uniform *n*-type extrinsic doping across the epitaxially grown structure, and taking into account the fact that the transition layer at the back interface is relatively thick (typically several microns, as indicated in Ref. 11), it would be expected that a higher sheet density will be observed for the E2 electrons, as evident in the experimental results shown in Fig. 5. This interpretation is consistent with the observations of Gui et al.,[13] who correlated Shubnikov–de Haas and QMSA measurements in LPE-grown HgCdTe ($x = 0.214$) at $T < 77$ K and reported three electron conductivity components associated with the bulk, and with the surface and the HgCdTe/substrate interfaces. Our observations are also in agreement with the three electron peaks reported at 100 K in LPE-grown *n*-type $Hg_{1-x}Cd_xTe$ layers ($x = 0.214$) in Ref. 14, wherein the high mobility carrier was associated with a bulk electron and the two lower-mobility carriers were assumed to be associated with surface and HgCdTe/substrate interfaces. Although additional measurements at lower temperatures, including measurements after surface etch-back, need to be undertaken to further confirm the above interpretation, it is important to note that the behavior of the mobility spectra described herein has not been previously reported.

While this study provides further evidence of the need for magnetic-field-dependent magnetotransport characterization and QMSA analysis to obtain the transport parameters of the individual carrier species present in HgCdTe epitaxial layers, this study also prompts the need for further studies on the effects of scattering mechanisms on the broadening of mobility spectrum distributions. To date, mobility spectrum broadening effects have not been studied largely due to: (a) the lack of robust mobility spectrum algorithms with sufficiently high

Table I. Selected transport parameters extracted from three LPE-grown HgCdTe *n*-type single layers

Sample	E_A E1 (meV)	E_A E2 (meV)	E_A E3 (meV)	$n_{E1(bulk)}$ at 95 K (10^{14} cm^{-3})	$\mu_{E1(bulk)}$ at 95 K (10^4 cm^2/Vs)	x; $E_{A(E1)}$	x; H&S
R2A	174 ± 13	21 ± 3	22 ± 2	8.3 ± 0.4	68.1	0.230 ± 0.009	0.239 ± 0.003
R3A	163 ± 19	20 ± 4	26 ± 2	12 ± 0.7	76.7	0.222 ± 0.013	0.234 ± 0.003
R3B	180 ± 21	21 ± 7	21 ± 5	12 ± 0.5	56.3	0.234 ± 0.015	0.237 ± 0.002

E_A, activation energy for E1, E2, and E3; $n_{E1(bulk)}$ at 95 K—concentration of E1; $\mu_{E1(bulk)}$ at 95 K—mobility of bulk electrons; x; $E_{A(E1)}$—composition from activation energy at high temperatures; x; H&S—composition from fit to Hansen and Schmit[12] expression.

resolution capable of resolving lines with variations as a function of temperature, and (b) the lack of theoretical models to describe conductivity-mobility spectrum line-width shape and thermal evolution.

CONCLUSIONS

Multicarrier transport studies were performed on three *n*-type LPE-grown HgCdTe samples using variable temperature and variable magnetic field. The experimental data analysis was undertaken using mobility spectrum techniques. Two algorithms were used, iQMSA and HR-QMSA, with the latter, recently developed technique demonstrating significantly better resolution, finer details, and better consistency in spectra evolution with changing temperature.

The three investigated samples demonstrated very similar transport parameters indicative of very high-quality material with high uniformity of HgCdTe material across the whole wafer. No contribution from holes was observed. In the electron spectra three carriers were identified. The dominant carriers can be attributed to the LWIR bulk absorbing layer, whereas the other two carriers are most likely associated with the wider-bandgap transition layer near the substrate and a surface accumulation layer.

This study provides further evidence for the need to undertake magnetic-field-dependent Hall-effect and resistivity measurements combined with mobility spectrum techniques in order to deconvolve the multicarrier transport parameters that are usually present in narrow-bandgap HgCdTe epitaxial layers. The extracted parameters provide invaluable information that can be readily used to improve the epitaxial growth process, especially in advanced multilayer structures.

ACKNOWLEDGEMENTS

The work presented in this paper has been supported by Raytheon Visions Systems, Raytheon Australia, and the Australian Research Council, as part of the ARC Linkage Project 0882537 “Development of an Advanced Semiconductor Characterization Capability for Infrared Focal Plane Array Applications.” The authors would like to express special thanks to J. Pellegrino, US Army NVESD, for his support of this project.

REFERENCES

1. A. Rogalski, J. Antoszewski, and L. Faraone, *J. Appl. Phys.* 105, 091101 (2009).
2. M.C. Gold and D.A. Nelson, *J. Vac. Sci. Technol. A* 4, 2040 (1986).
3. W.A. Beck and J.R. Anderson, *J. Appl. Phys.* 62, 541 (1987).
4. Z. Dziuba and M. Gorska, *J. Phys. III* 2, 110 (1992).
5. J. Antoszewski, D.J. Seymour, L. Faraone, J.R. Meyer, and C.A. Hoffman, *J. Electron. Mater.* 24, 1255 (1995).
6. I. Vurgaftman, J.R. Meyer, C.A. Hoffman, D. Redfern, J. Antoszewski, L. Faraone, and J.R. Lindemuth, *J. Appl. Phys.* 84, 4966 (1998).
7. S. Kiatgamolchai, M. Myronov, O.A. Mironov, V.G. Kantser, E.H.C. Parker, and T.E. Whall, *Phys. Rev. E* 66, 036705 (2002).
8. J. Antoszewski, L. Faraone, I. Vurgaftman, J.R. Meyer, and C.A. Hoffman, *J. Electron. Mater.* 33, 673 (2004).
9. J. Rothman, J. Meilhan, G. Perrais, J.-P. Belle, and O. Gravrand, *J. Electron. Mater.* 35, 1174 (2006).
10. G.A. Umana-Membreno, J. Antoszewski, and L. Faraone, HR-QMSA algorithm and software, The University of Western Australia (unpublished).
11. M.H. Kalisher, P.E. Herning, and T. Tung, *Prog. Cryst. Growth Charact.* 29, 41 (1994).
12. G.L. Hansen and J.L. Schmit, *J. Appl. Phys.* 54, 1639 (1983).
13. Y.S. Gui, G.Z. Zheng, J.H. Chu, S.L. Guo, X.C. Zhang, D.Y. Tang, and Y. Cai, *J. Appl. Phys.* 82, 5000 (1997).
14. J. Chu and A. Sher, *Physics and Properties of Narrow Gap Semiconductors*, Chap. 5 (New York: Springer, 2008), pp. 457–462.